IEEE Access
Multidisciplinary ⋮ Rapid Review ⋮ Open Access Journal

Received 9 July 2024, accepted 19 August 2024, date of publication 28 August 2024, date of current version 6 September 2024.

Digital Object Identifier 10.1109/ACCESS.2024.3450868

RESEARCH ARTICLE

Frequency and Pattern Reconfigurable CPW-Fed MIMO Antenna With Multiband and Wideband Characteristics

ADAMU HALILU JABIRE[1,2], (Member, IEEE), HAMAD M. ALKHOORI[1], (Member, IEEE), ADNAN GHAFFAR[3], YANAL S. FAOURI[4], (Senior Member, IEEE), ABDULRAHMAN DAHIR[1], AND MOUSA I. HUSSEIN[1], (Senior Member, IEEE)

[1]Department of Electrical and Communication Engineering, United Arab Emirates University, Al Ain, United Arab Emirates
[2]Department of Electrical and Electronics Engineering, Taraba State University, Jalingo 660213, Nigeria
[3]Department of Electrical and Electronics Engineering, Auckland University of Technology, Auckland 1010, New Zealand
[4]Electrical Engineering Department, The University of Jordan, Amman 11942, Jordan

Corresponding author: Mousa I. Hussein (mihussein@uaeu.ac.ae)

This work was supported by United Arab Emirates University.

ABSTRACT This study introduces a coplanar waveguide MIMO antenna design that offers both frequency and pattern reconfigurability. The antenna is intended for applications in WiMAX, WLAN, and X-Band. It is constructed using an FR4 substrate with dimensions of 1.6mm thickness and 0.025 loss tangent. Based on the proposed design, MIMO antennas can operate at 3.5 & 3.9GHz (WiMAX), 5.5 & 5.8GHz (WLAN) and 10.5 & 12.5GHz (X-Band). To accomplish this, two open-circuited 3mm x 3mm quatre wavelength transformers are linked to each radiator through PIN diodes. The performance enhancement of the reconfigurable MIMO antenna was fine-tuned utilizing microwave solvers in both CST and ADS. The system's performance was validated through practical measurements. Furthermore, the analysis of diversity conducted on the suggested antenna reveals that the antenna has a low correlation coefficient (< 0.0001), channel capacity (< 0.4bits/sec/Hz), and total active reflection coefficient (< 0dB). The measured isolation of < -20dB is noticed for all three states. Antenna peak gain is 6.2dBi, with over 80% efficiency. A MIMO antenna with these characteristics suits a wide range of wireless communication systems.

INDEX TERMS Coplanar waveguide, equivalent circuit, multiple-input-multiple-output (MIMO), multi-band, positive intrinsic negative (PIN) diode.

I. INTRODUCTION

The fast technology-advancing world constantly pushes the efficiency boundaries of a provided service to be enhanced, resulting in the development of new tools. Radiofrequency (RF) systems are expected to be frequency agile, cognitive, and software-defined to enable optimum spectrum and power utilization [1]. This system requires antenna architectures that are reconfigurable and multifunctional. Frequency reconfiguration reorganizes the electrical length of the radiator and requires additional passive components to reconfigure the operating frequency bands. The most desired capabilities for antennas include reconfiguration in an active frequency band, radiation pattern, and polarization while occupying minimal space. Antenna reconfiguration is typically achieved by deliberate rearrangement of individual components, including radiating components, feed networks, or parasitic elements in the vicinity of the antenna [2]. Ideally, when one antenna property is reconfigured, the other desirable properties should remain unchanged. Obtaining reconfiguration in one antenna property is challenging without negatively impacting other desirable properties. The reconfigurable and MIMO antenna are two different things; synergizing the features will help enhance the two techniques. The two techniques need to be merged to benefit from MIMO and reconfigurability, leading us to dynamically improve the system performance in

The associate editor coordinating the review of this manuscript and approving it for publication was Julien Sarrazin.

a changing scenario compared to a conventional wireless system. As a result, antennas are required to have frequency tuning features to adapt some useful frequency bands. Thus, reconfigurable antennas become a unique solution in wireless communication to incorporate multimode functionality in a single aperture rather than a fixed instrument [3] [4] [5]. Hence, a reconfigurable frequency antenna can perform best in a wireless communication system. Antennas must have frequency tuning features to conform newly released frequency bands with other sub-6GHz bands [6].

Antenna reconfiguration techniques include PIN diodes [7], [8], varactor diodes [9], radio frequency microelectromechanical systems (RF-MEMS) [10] [11] [12], optical techniques [13], [14], smart materials [15], [16], and mechanical techniques [16], [17]. In [18], a UWB-MIMO antenna was reported with a bandwidth of 1.48-4.56GHz and the ability to operate on multiband; however, the antenna design was complex. In [19], a reconfigurable MIMO antenna for WLAN and UWB applications has been reported. The gain is relatively high, but the isolate. In [20], a reconfigurable MIMO antenna for UWB has been reported. Although it has a relatively high gain, the antenna is not compact. The narrow open-slot LTE-MIMO antenna reported in [21] is capable of multiband operation at the lower band of GSM and LTE. Despite this, the antenna has low isolation and efficiency. According to [22], PIN diodes can switch parasitic ground structures over four frequencies. It is, however, a complex design. A circular patch MIMO antenna with reconfigurability, aimed at 5G sub-6GHz and WLAN applications, is documented in reference [23]. Operating in a dual-band of 3.4 – 3.8GHz, this antenna demonstrates a maximum gain of 2.68dBi. Its drawback lies in its low gain and efficiency. In another study, a frequency-agile MIMO antenna, outlined in [24], employs a reconfigurable feedline. While offering an impedance range of 1.42 – 2.27GHz, it contends with low gain and occupies more space. Meanwhile, [25] presents a multimode frequency-reconfigurable MIMO antenna catering to sensing and reconfigurable communication modes. Despite its broader functionality, the antenna lacks compactness and features a relatively modest gain of 2.6dBi. A separate instance of a circular patch MIMO antenna for 5G sub-6GHz and WLAN applications, as described in [23], also uses the dual-band from 3.4 to 3.8GHz. A compact reconfigurable MIMO antenna, outlined in [26], is designed for WLAN and WiMAX-band microwave sensing. Employing four PIN diodes for reconfiguration, this antenna boasts multiband frequency response and compact dimensions yet faces limitations regarding gain and bandwidth. A different approach is seen in [27], where a frequency-reconfigurable yagi-like MIMO antenna employs varactor diodes for switching. Its wideband response covers 2.5 – 4.5GHz, with a commendable gain of 5dBi, but its compactness is compromised.

The horn bowtie dumbbell antenna incorporates a machine-learning technique to achieve pattern reconfigurability, as detailed in [28]. By positioning three PIN diodes within the gaps of the reflector and manipulating their states, a significant alteration in the radiation pattern is achieved, enabling the adjustment of beam width from 10.70 to 156.20. In a different approach, [29] presents a configurable antenna array of dimensions 1×4, offering both broadband frequency tuning and a wide scanning angle. This innovation is based on octagon microstrip patches, allowing for simultaneous configuration of frequency and far-field pattern. Another reconfigurable pattern antenna is highlighted in [30], where liquid metal is the core element. A balun feeds the dipole, and the adaptability to modify the length of the parasitic dipoles results in configurable radiation characteristics. Likewise, [31] introduces an inventive antenna with adaptable patterns, utilizing a low-profile electric and magnetic radiation source for diversified patterns under 6GHz. Pattern adjustments are facilitated by the integration of PIN diodes in the reconfigurable network. This arrangement facilitates eight radiation modes for beam steering, spanning a full 360-degree range.

The above literature illustrates the wide range of reconfigurable MIMO antennas used in WiMAX, LTE, ISM, WLAN, and 5G sub 6GHz applications. Although some antennas are compact in size, simple geometry, and design, they have relatively low gain, narrow bandwidth, and low isolation. Though some designs may have higher gain and high isolation, their disadvantage is complex structure and non-compactness, and a product like this can be costly to manufacture. Based on the above study, a wide band and compact reconfigurable MIMO antenna should be created using simple geometry, as well as being small and having high gain and isolation. A part from that, the proposed antenna has both frequency and pattern reconfigurabilty. Which find application in wireless communication system, MIMO systems, IOT and mobile devices. This study proposes an antenna of the same kind constructed using a simple and cost-effective substrate. PIN diodes can be used to set it for use over a wideband covering sub-6GHz applications, such as WLAN, WiMAX, 4G, 5G, and X-band. In the rest of the letter, four sections are presented. Section II explores the MIMO antenna design process, the suggested antenna's form, its operational principle, and the equivalent circuit model. In section III, the measured results and the hardware prototype are discussed. The diversity analysis and comparison of the suggested MIMO antenna with the most recent research are covered in section IV. Section V concludes with final remarks.

II. THE PROPOSED MIMO RECONFIGURABLE ANTENNA DESIGN METHODOLOGY

A. MIMO ANTENNA CONFIGURATION

The proposed geometry of a reconfigurable MIMO system is shown in Figure 1. The W1 is used to excite the antenna's stepped radiators, which has the benefit of having wideband characteristics. Two open-circuited quatre wavelength transformers are coupled to stepped rectangular radiators via

PIN diodes D1, D2, D3, and D4 for frequency and pattern reconfigurability. Modifying the distance between the feedline and the ground plane matches the proposed antenna to 50Ω feedlines. A common ground plane is connected via L6, as depicted in Figure 1. On the top side of an FR4 substrate with a loss tangent of 0.025, relative permittivity of 4.3, and thickness of 1.6mm, the MIMO antenna is etched. The antenna's performance was optimized using Advanced Design System (ADS) and Computer Simulation Technology (CST). Table 1 displays the optimal parameters of the suggested antenna.

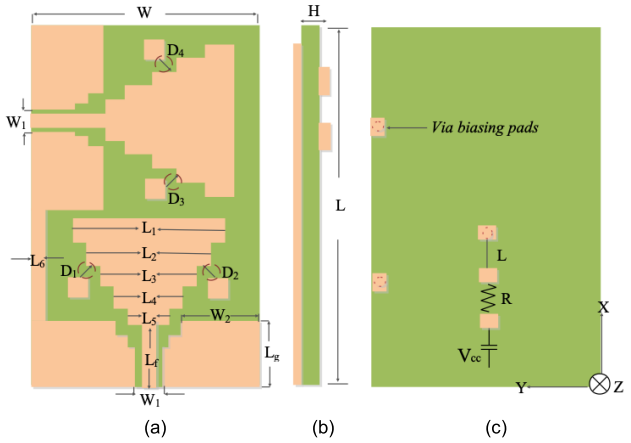

FIGURE 1. The proposed CPW-fed frequency and pattern reconfigurable MIMO antenna's geometry is (a) front view, (b) side view, and (c) back view.

TABLE 1. Dimensions of the proposed configurable MIMO antenna.

Parameter	Dimension (mm)	Parameter	Dimension (mm)
L	32	L_6	1
L_1	8	L_f	11
L_2	4	L_g	12.5
L_3	2.5	W	26
L_4	2.5	W_1	2.8
L_5	2	W_2	11.3

B. EVOLUTION STEPS

The stages that were necessary to complete the development of the CPW-fed rectangular monopole antenna are depicted in Figure 2(a). The MIMO antenna was designed using a 7GHz center frequency. The S_{11} spectra of the MIMO antenna in Fig. 2(b) are limited. When a rectangular patch is added to the second stage on top of the initial radiator, the S11 response experiences a further enhancement in the lower band. In the third step, a rectangular patch of different lengths and widths is added to the top of the second patch. This step, as seen in Fig. 2(b), greatly enhances the S_{11} response, while it is not precisely matched. In the fourth step, the additional stepped rectangular patch is attached. This resulted in introducing two wideband frequency modes starting from 2.7 – 5.8GHz and 8 – 11.5GHz, and an impedance match of more than -30dB & -15 dB. The fifth phase involves the addition of an additional rectangular patch atop the fourth one. This new patch enhances the antenna's capabilities, resulting in a UWB response spanning 2.8 – 12 GHz. The The foundation of the suggested antenna is rooted in the fifth step. To achieve reconfigurable architecture, the quatre wavelength transformer remains linked to the primary radiator via PIN diode switches, which can be toggled between the "on" and "off" states. The quatre wavelength transformer is 3mm × 3mm, calculated using equation (1).

$$\frac{\lambda_6}{4} = \left[\frac{C}{\sqrt{\varepsilon_{eff}} \times f}\right] \tag{1}$$

where c = 3 × 10^8m/s is the speed of light, f = 6 GHz, and ε_{eff} = 4.3.

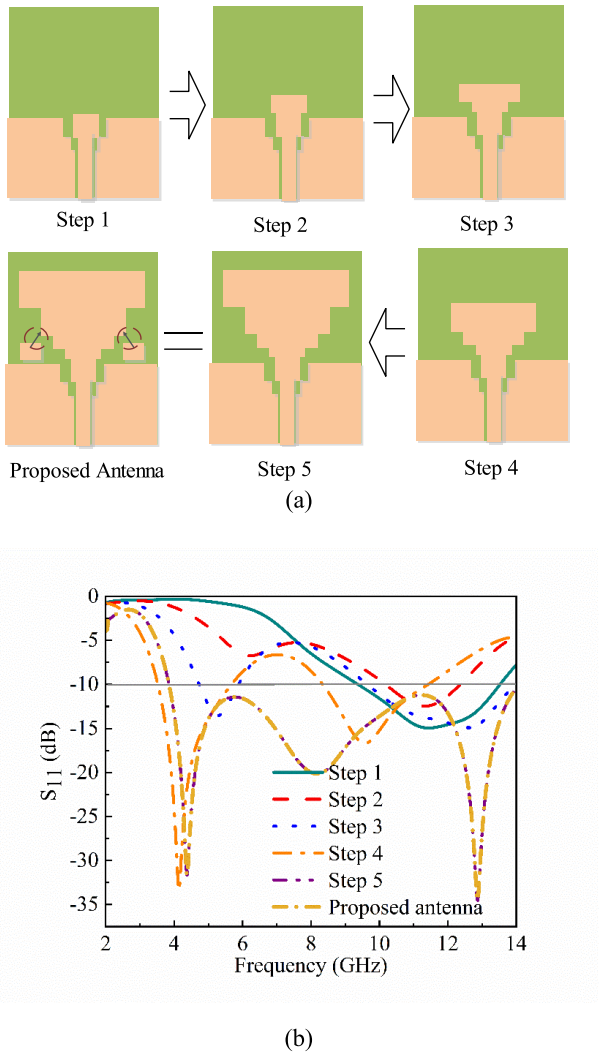

FIGURE 2. (a) Evolution stages of suggested MIMO antenna, (b) S11 spectra of the various stages.

C. EQUIVALENT CIRCUIT MODEL ANALYSIS

1) EQUIVALENT CIRCUIT FOR CASE-00 (OFF STATE)

The ADS software was utilized to optimize the equivalent circuit of the proposed MIMO antenna when it's in its

off state, as depicted in Figure 3. The basis to choose the value of resistance is based on the use of lumped elements from the ADS software and assigning a certain range of values from the simulation variable setup of 1 × 10^-6 to 1.5 × 10^6 which is large enough for convergence during the optimization process. The gradient optimization technique is employed to refine the model parameters within the specified range of minimum and maximum values for each component [32]. The model consists of connections between the feedline's first parallel RLC circuit and an inductor on the left-hand side representing the first port, followed by four cascaded RLC circuits with a second inductor for the second port. Two inductors, L_{f3} and L_{f4}, in series with two parallel shunt capacitors 0.15pF that represent the four diodes in their off states. The graphical representation of the S_{11} spectra is illustrated in Figure 4, showcasing a comparison with the full-wave CST model, which enables two narrow bands of 2.8GHz & 3.5GHz, and two ultra-wideband response of 4.8 – 7GHz & 9 -13GHz, respectively. The optimized circuit components are given in Table 2.

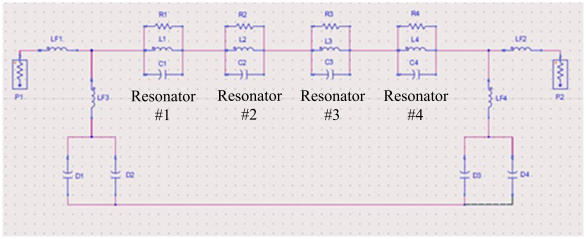

FIGURE 3. Equivalent circuit model for case-00 (off-state).

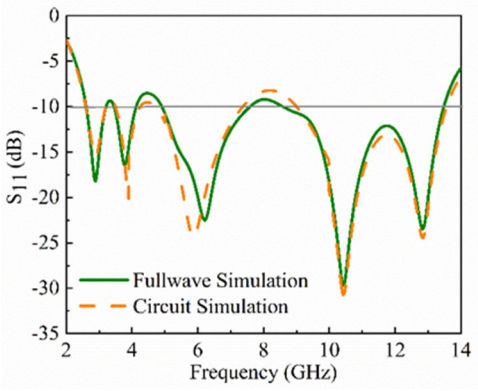

FIGURE 4. Equivalent circuit model S11 for case-00 (off-state).

TABLE 2. Components used in case-00 (off state), (R(Ω), L(pH), C(pF)).

$R_1 = 60.77$	$R_2 = 32492$	$R_3 = 47.85$	$R_4 = 25217$
$L_1 = 260.2$	$L_2 = 9.001$	$L_3 = 397.1$	$L_4 = 285.9$
$C_1 = 1.382$	$C_2 = 1.263$	$C_3 = 5.933$	$C_4 = 4.624$
$L_{F1} = 668.6$	$L_{F2} = 40.32$	$L_{F3} = 315.3$	$L_{F4} = 118$
$D_1 = 0.15$	$D_2 = 0.15$	$D_3 = 0.15$	$D_4 = 0.15$

2) EQUIVALENT CIRCUIT FOR CASE-01 (ON STATE)

A similar analysis was performed for a proposed configurable MIMO antenna. The diode is activated, and the four shunt capacitors are replaced with four 1.5Ω resistors. The values of the circuit parameters are re-optimized to produce a wide impedance width from 2.7 – 4GHz, 6 – 8GHz and 9 – 11.5GHz. The equivalent circuit of the diodes status is shown in Figure 5, four sections of parallel RLC resonators have been utilized to represent the UWB behavior of the designed antenna, the more resonators the more the bandwidth [32]. The effect of adding one resonator at a time is shown in Figure 6b, after adding each resonator a wide optimization has been conducted to predict the components values. The four resonator case match the antenna behavior with the optimized parameters have been determined using ADS simulator. The refined parameter values for the circuit components are detailed in Table 3.

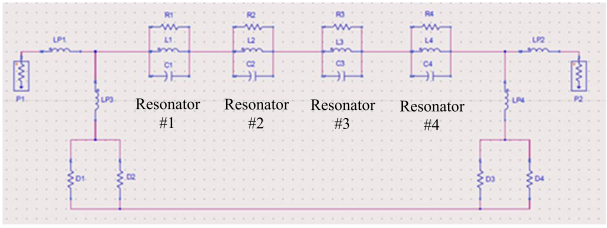

FIGURE 5. Equivalent circuit model for case-01 (on-state).

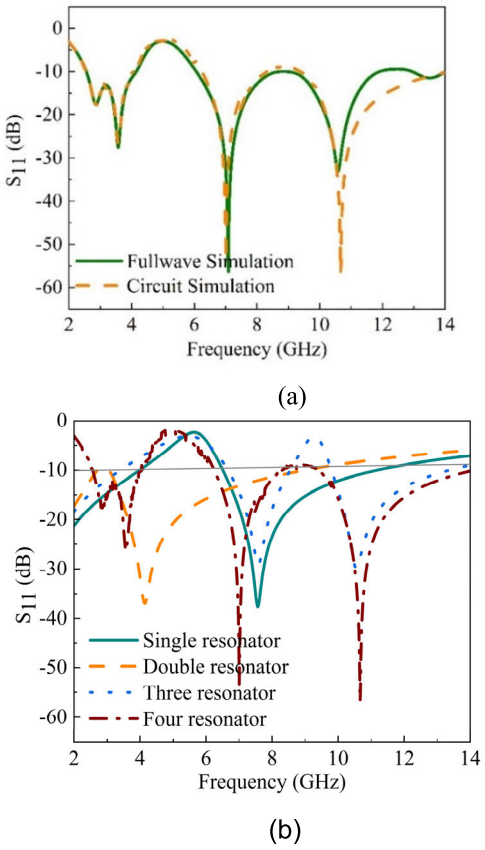

FIGURE 6. (a) Equivalent circuit model S11 for case-01 (on-state), (b) S11 responds for various resonators.

TABLE 3. Components used in case-01 (on state), (R(Ω), L(pH), C(pF)).

$R_1 = 0.005$	$R_2 = 11284$	$R_3 = 62054$	$R_4 = 34840$
$L_1 = 14216$	$L_2 = 0.9361$	$L_3 = 0.1005$	$L_4 = 14725$
$C_1 = 0.023$	$C_2 = 1.6690$	$C_3 = 3.4340$	$C_4 = 1.6250$
$L_{P1} = 1.424$	$L_{P2} = 621.6$	$L_{P3} = 951.8$	$L_{P4} = 1.045$
$D_1 = 4.5$	$D_2 = 4.5$	$D_3 = 4.5$	$D_4 = 4.5$

3) EQUIVALENT CIRCUIT FOR CASE-02 (OFF, ON, ON, OFF STATE)

Further optimization processes were performed on the components shown in Figure 7 to see the effect on the S_{11} spectra. In this state, the first resistor is replaced with a shunt capacitor in the first diode. For the fourth diode, the resistor is also replaced with one shunt capacitor representing the "OFF, ON, ON, OFF" state after the four cascaded RLC circuits, which produce a single wideband and one ultra-wideband at 2.7 – 4.2GHz and 6 – 11GHz respectively. Figure 8 depicts the MIMO model S_{11} as compared to the CST model. The optimized values of the circuit parameters are given in Table 4.

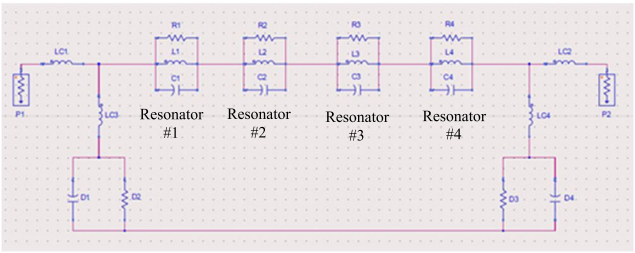

FIGURE 7. Equivalent circuit model for case-02 (off, on, on, off-state).

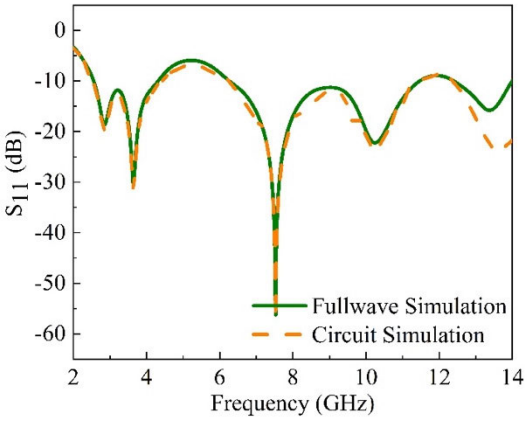

FIGURE 8. Equivalent circuit model S11 for case-02 (off, on, on, off-state).

4) CIRCUIT MODEL PARAMETRIC ANALYSIS

Some circuit components have undergone an optimization process to examine the effects on antenna responses and the critical effect components. Varying the resistor 'R_4' values will impact the antenna in terms of its matching around 2.8GHz, 7GHz, and 10 – 14GHz. The value of the 'R_4' for 1Ω, 3.481Ω, 135.8Ω and 3484.5Ω are visualized in Figure 9(a); as the resistance increases, achieving S11 matching becomes possible. The optimal value is 3484.5Ω. The second investigated component is 'L_2'. Its effect is depicted in Figure 9(b) around 2.8GHz, 7GHz, and 10.7GHz. The impact of capacitance 'C4' on enhancing the matching of the proposed antenna is explored in Figure 9(c). As the capacitance value rises, the frequency alignment also increases.

TABLE 4. Components used in case-02 (off, on, on, off state), (R(Ω), L(pH), C(pF)).

$R_1 = 47942$	$R_2 = 47.93$	$R_3 = 361.0$	$R_4 = 50.21$
$L_1 = 413.0$	$L_2 = 26.02$	$L_3 = 1.231$	$L_4 = 51.01$
$C_1 = 2.150$	$C_2 = 78.63$	$C_3 = 4.399$	$C_4 = 3.31$
$L_{C1} = 3230$	$L_{C2} = 17.9$	$L_{C3} = 216$	$L_{C4} = 634$
$D_1 = 0.15$	$D_2 = 4.5$	$D_3 = 4.5$	$D_4 = 0.15$

D. PRINCIPLE OF OPERATION

Four PIN diodes, $D_1 – D_4$, are coupled to two open-circuited transformers; when $D_1 – D_4$ are activated in forward DC bias mode, the lower rectangular monopole antenna radiates. As explained below, the four PIN diodes offer different biasing scenarios.

1) CASE-00

The four diodes in this instance are reverse-biased (switch OFF). Hence, the MIMO antenna radiates at 2.8GHz, 3.5GHz, 4.9 – 7.6GHz and 8.6 – 13.4GHz. In this case, adding a biasing circuit does not affect S11, as depicted in Figure 10.

2) CASE- 01

The four PIN diodes D_1 through D_4 in this instance are forward-biased (switch ON), thus connected to the main radiator. This antenna configuration, therefore, resonates at (2.5 – 4.16GHz, 6.1 – 8.5GHz, and 9.1 – 11.8GHz) bandwidths. The effect of adding a biasing circuit affected the S_{11} in this second case, as depicted in Figure 11.

3) CASE-02

Diode D_1 is reverse-biased (switched off) in this last scene, while D_2 and D_3 are forward-biased (switched on), and D_4 is reverse-biased (switched off). In this situation, the antenna radiates at frequencies between 2.56 - 4.3 GHz, 6.3 - 11.4 GHz, and 12.4 - 14 GHz. Figure 12 depicts the S_{11} after adding the biasing circuit.

III. MEASURED AND SIMULATION RESULTS

This section demonstrates the simulated and measured results of the proposed reconfigurable MIMO antenna. The RF PIN diode employed in the proposed MIMO antenna's equivalent circuit model is shown in Figure 13 for both forward bias (switch on) and reverse bias (switch off) conditions. The experimental setup is depicted in Figure 14, while Figure 15 showcases the constructed antenna. The MIMO antenna's S_{11} spectra and isolation capabilities were evaluated using a

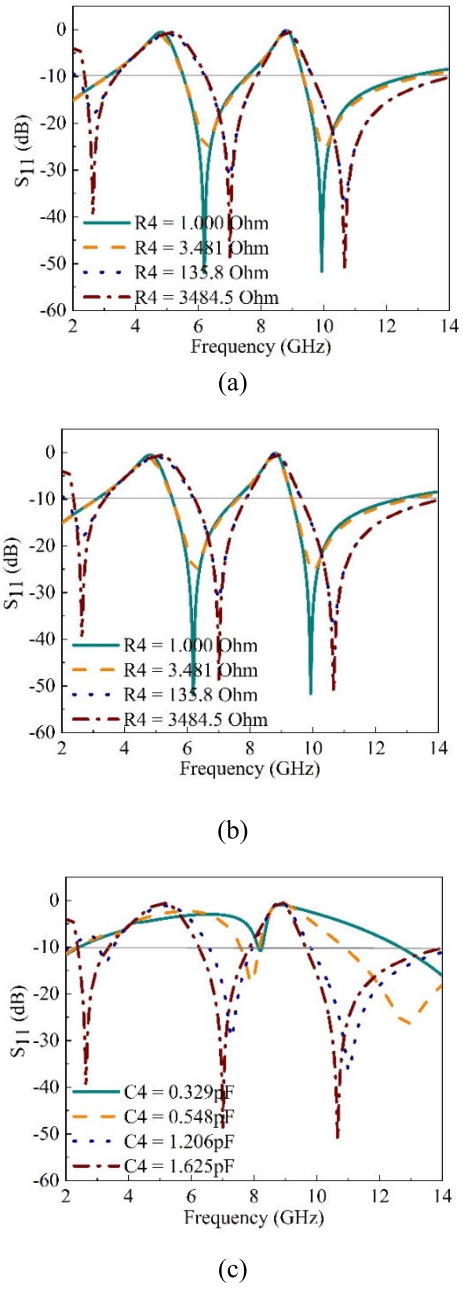

FIGURE 9. Optimization of the circuit components when the diodes are all ON (a) R4, (b) L2, and (c) C4.

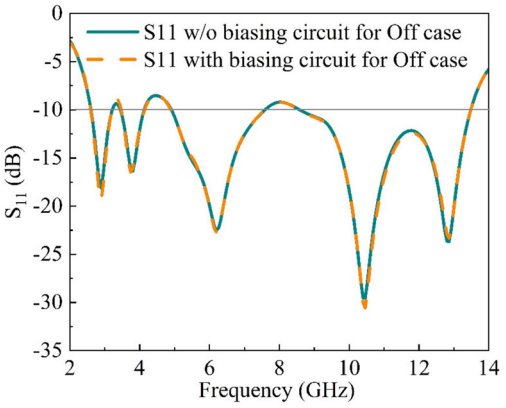

FIGURE 10. The effect of a biasing circuit for OFF state.

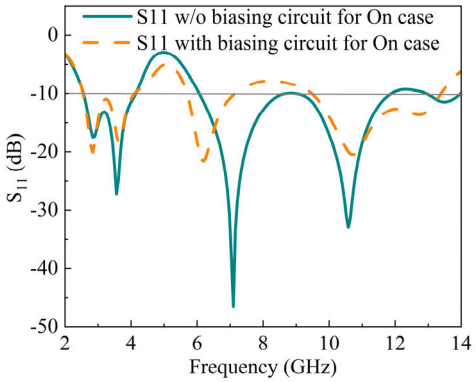

FIGURE 11. The effect of a biasing circuit for ON state.

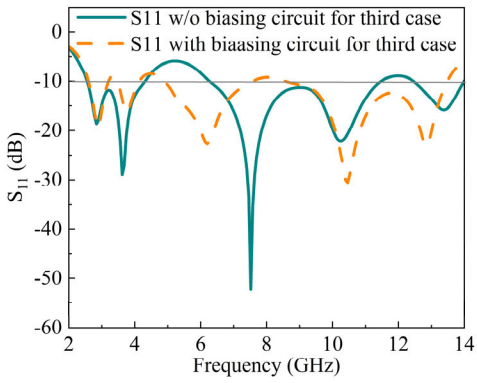

FIGURE 12. The effect of a biasing circuit for OFF, ON, ON-OFF state.

vector network analyzer (ROHDE & SCHWARZ ZVL VNA model) covering the frequency range of 9kHz to 13.6GHz. An anechoic chamber (Model 6000, S/N 2019017) was utilized to measure far-field patterns. Reception was facilitated by a standard horn antenna, maintaining a 1-meter separation between the test antenna and the reference horn antenna. Only three cases were reported because all the remaining thirteen states were analyzed, but there were no changes with respect to the states.

A. CASE-00

When both PIN $D_1 - D_4$ are turned off, the S_{11} and S_{21} spectra, realized gain and total efficiency are shown in Figure 16. Indicating that the suggested antenna resonates at 2.8GHz, 3.5GHz narrow bandwidth, wide impedance width of 4.9 – 7.6GHz and 8.6 – 13.4GHz. The peak realized gain is >5dBi at 11GHz, and the peak measured efficiency is > 80%, ranging from 3GHz to 15GHz. The simulation results align well with the measurement data.

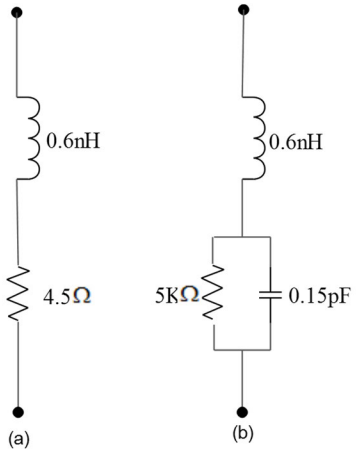

FIGURE 13. The equivalent circuit for the PIN diode is (a) forward-biased and (b) reverse-biased.

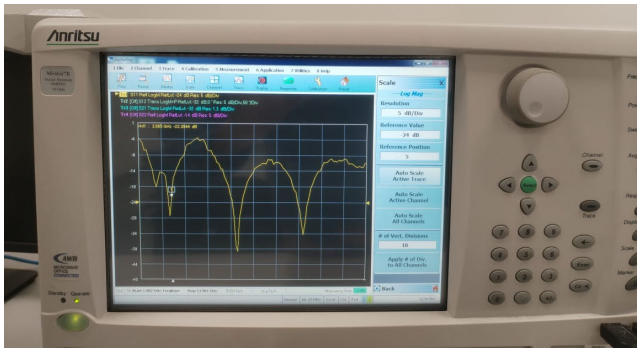

FIGURE 14. Experimental setup for CPW-fed configurable MIMO antenna at On state.

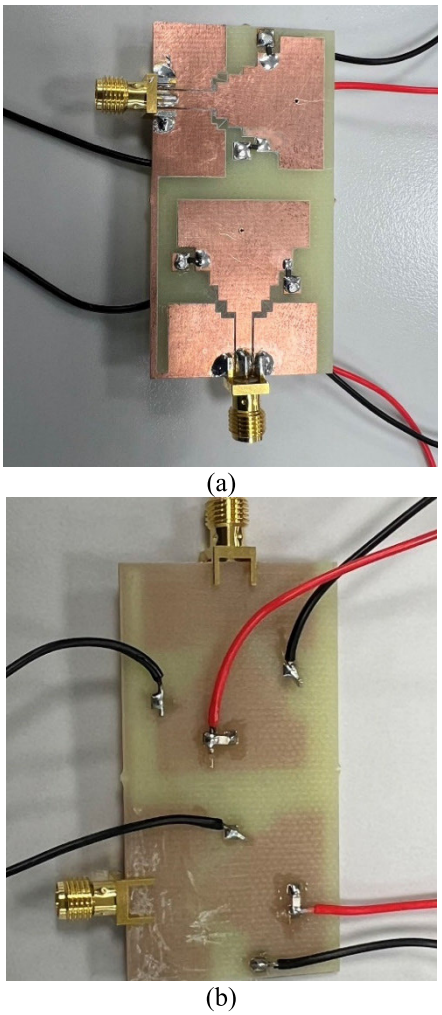

FIGURE 15. Prototype of the proposed frequency and pattern configurable MIMO antenna (a) front view, (b) back view.

B. CASE-01

The measured and simulated (S_{11} & S_{21}), peak realized gain, and MIMO antenna's efficiency when D_1 through D_4 are in the ON state is depicted in Figure 17. In this configuration modes, three wideband resonance frequencies have been realized, i.e., 2.5 – 4.6GHz, 6.1 – 8.5GHz and 9.1 – 11.8GHz respectively. The measured peak realized gain is 6.2dBi at 13.4GHz. The measured peak efficiency is 81% at 8.6GHz. The simulation results align well with the measurement data.

C. CASE-02

Figure 18 presents the spectral profiles of S_{11} and S_{21}, as well as the gain and radiation efficiency of the proposed MIMO antenna across four distinct switching conditions: D_1 off, D_2 on, D_3 on, and D_4 off. In this case, the antenna resonates at three different wideband responses of 2.56 – 4.3GHz, 6.3 – 11.4GHz, and 12.4 – 14GHz. Both measured and simulated isolations are below -30 dB. The highest efficiency, reaching 83.2% at 9.2 GHz, corresponds to a peak realized gain of 4.7 dBi at 11 GHz. Consistency between simulation and measurement is evident. In Table 5, the performance of the MIMO antenna is detailed under various PIN diode switching conditions. It is significant to observe that the antenna consistently upholds intense isolation levels below -20 dB, attains peak gains exceeding four dBi, and sustains a radiation efficiency surpassing 80%. The information provided in the table underscores the proposed MIMO antenna's flexibility for diverse applications, such as WLAN, WiMAX, and X-band, as it can be electronically adjusted.

TABLE 5. Performance of an antenna when subjected to different switching scenarios involving PIN diodes.

Case	Mode of operation	Measured Band (GHz)	Peak gain (dBi)	Efficiency (%)
00	Multiband	2.8, 3.5, 4.9-7.6, 8.6-13.4	5	80
01	Wideband	2.5-4.6, 6.1-8.5, 9.1-11.8	6.2	81
02	Wideband	2.56-4.3, 6.3-11.4,12.4-14	4.7	83.2

D. FAR-FIELD PATTERN RECONFIGURABILITY

The radiation mechanism of the antenna elements is based on the excitation of surface currents on the patch and

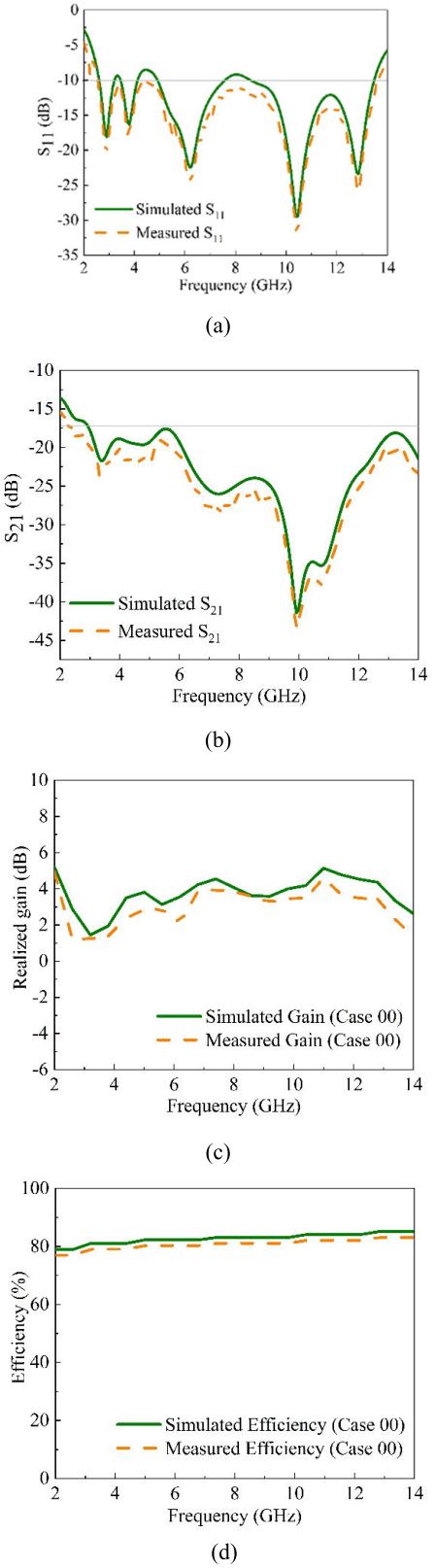

FIGURE 16. The spectral profiles of S11 and S21 realized gain and efficiency for the suggested MIMO antenna under the condition where both PIN diodes are reverse biased (switched off).

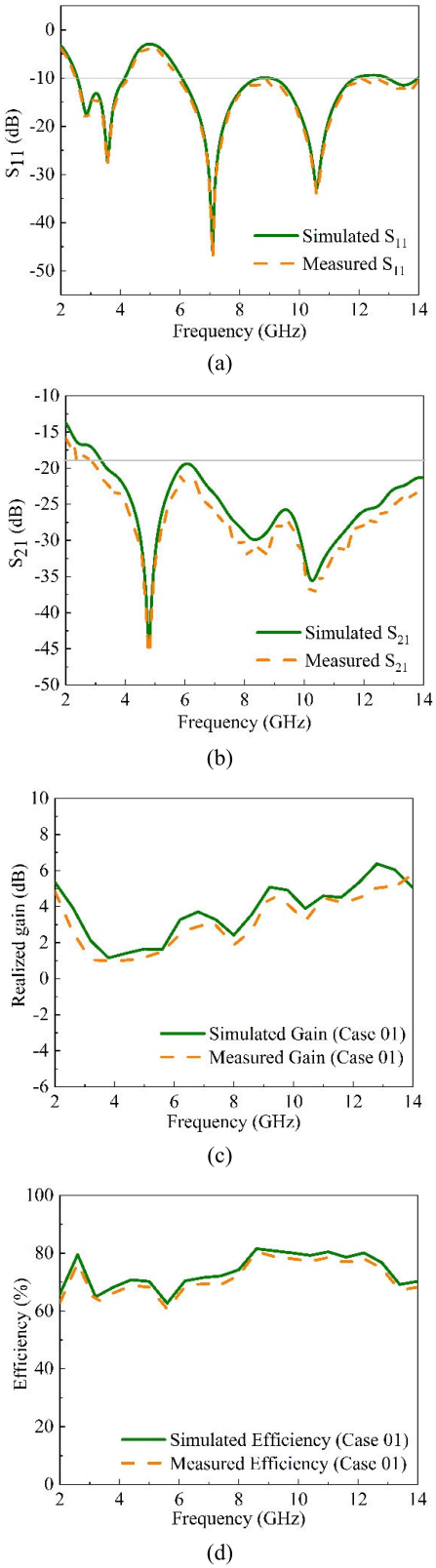

FIGURE 17. Spectral characteristics of S11, S21, gain, and efficiency for the suggested MIMO antenna under the condition where both PIN diodes are biased forward (turned on).

the subsequent radiation of electromagnetic waves. In this design, the antenna elements are optimized for frequency and pattern reconfigurability, which is achieved through specific geometric configurations and the inclusion of slots and vias.

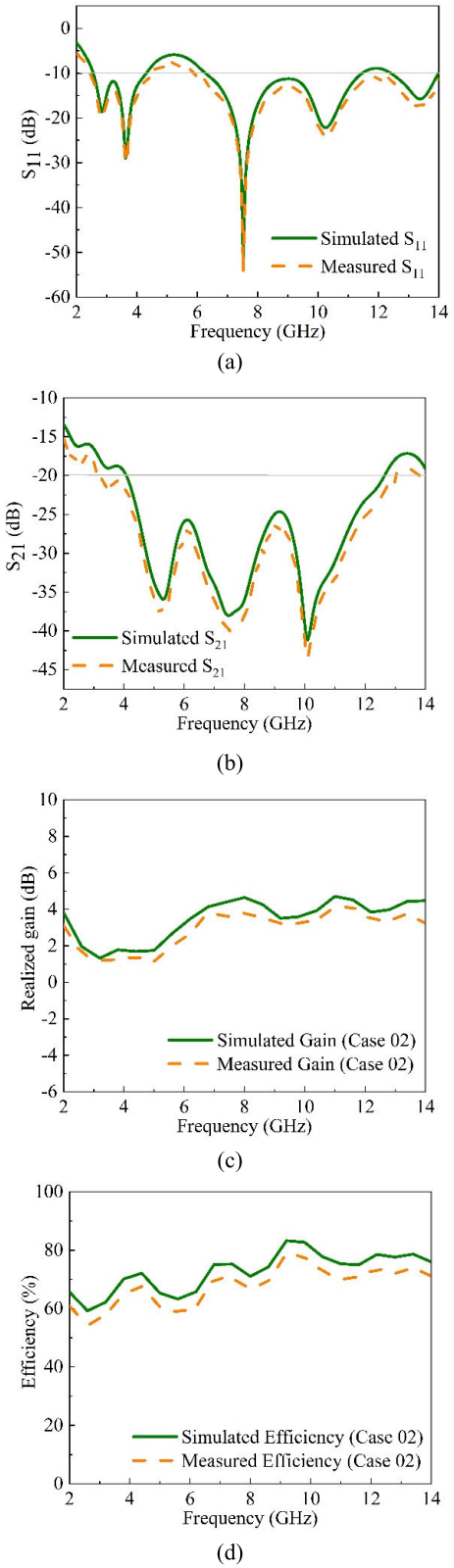

FIGURE 18. The S11 spectra and S21 spectra realized gain and efficiency response when the diodes are in the OFF, ON, ON, and OFF modes.

When the antenna is fed with a signal, surface currents are induced on the patch. These currents create electromagnetic fields that radiate away from the antenna. The distribution of the surface current is influenced by the shape and dimensions of the radiator, as well as the presence of slots and vias. The antenna was subjected to measurement within a calibrated anechoic chamber to assess its far-field radiation characteristics, illustrated in Figure 19. The prototype that was fabricated was placed atop a rotating platform, facing a wideband horn antenna positioned at a distance of 1 meter. The diodes were regulated using a DC source set at 6.8V according to the datasheet specifications. Figure 20 exhibits a measured radiation pattern of the antenna for the PIN diodes in state 00-02 at a frequency of 2.8GHz, observing both the E-plane and H-plane. The MIMO antenna at 2.8GHz showcases omnidirectional patterns in the E-plane during the OFF state, exhibiting a slight tilt in the ON state, and a broadside direction is observed for the OFF-ON-ON-OFF configuration. In the H-plane, radiation occurs in two opposite directions for the OFF-OFF states, while for the case of 02, the pattern displays bidirectional characteristics.

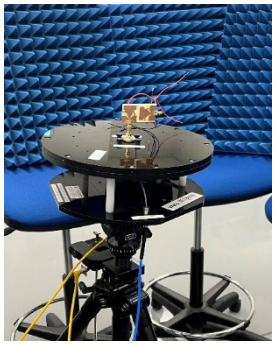

FIGURE 19. The proposed configurable MIMO antenna's far-field setup.

For cases 00 to 02 at 3.5GHz and 5.8GHz, the E-plane showed a broadband pattern, while the H-plane displayed a bidirectional pattern. Figures 21 and 22 illustrate this. The E and H planes also exhibit a different pattern when the antenna is in case 00 – case 02 at 10.5GHz, as shown in Figure 23. There is excellent agreement between the measured and simulated far-field patterns for diodes in OFF, ON, and OFF, ON, ON, OFF states.

The configurable MIMO antenna's surface current density was investigated when both port one and port 2 were excited. Figure 24 presents the surface current density at 2.8GHz, 3.5GHz, 5.8GHz and 10.5GHz, respectively, when port 1 is excited. Similar plots were obtained when port 2 was excited as shown in Figure 25. An input port experiences a more pronounced accumulation of currents. The majority of these currents were centered around the feedlines and the tips of the patch antenna.

IV. RECONFIGURABLE MIMO ANTENNA DIVERSITY ANALYSIS

This section analyzes and discusses the MIMO metric performance of the suggested antenna. In our proposed design, we did not use any decoupling network because there is

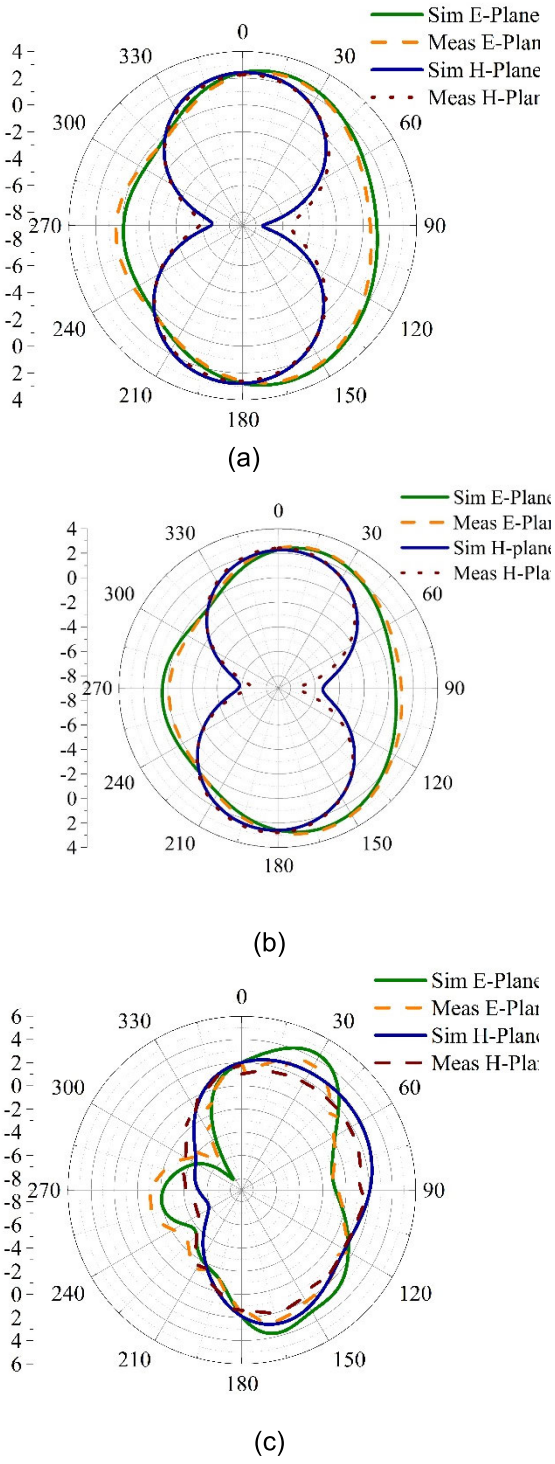

FIGURE 20. Simulation and measurement pattern reconfigurability at 2.8GHz (a) case-00, (b) case-01, and (c) case-02.

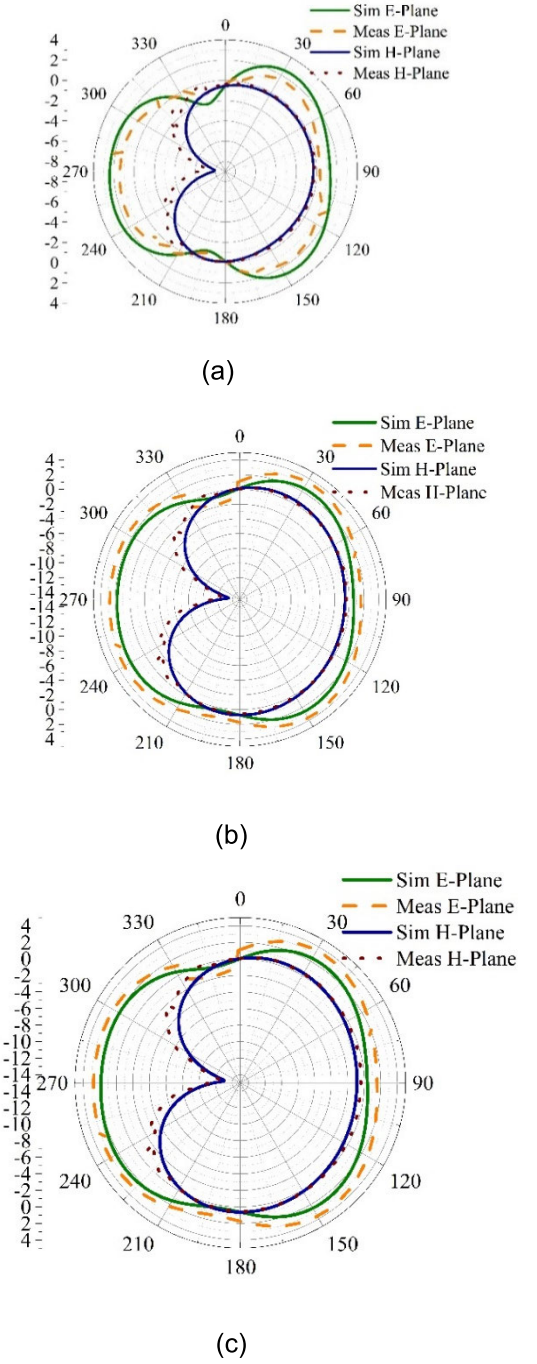

FIGURE 21. Simulation and measurement pattern reconfigurability at 3.5GHz (a) case-00, (b) case-01, and (c) case-02.

a quadrature phase shift of the two antenna orientations. A parametric analysis is carried out for different distances between the two antenna elements, which shows the effect in the isolation of the reported antenna, as depicted in Figure 26, where the optimum value has been selected. There are several ways to quantify performance, including measuring the total active reflection coefficient (TARC), the envelope correlation coefficient (ECC), the channel capacity loss (CCL), the diversity gain (DG), and the mean effective gain (MEG). TARC quantifies signal interference between MIMO channels. It was calculated using the following equation (2) [33]:

$$TARC = \frac{\sum_{n=1}^{N} |b_i|^2}{\sum_{n=1}^{N} |a_i|^2} = \sqrt{\frac{\left(S_{ii} + S_{ij}\right)^2 + \left(S_{jj} + S_{ji}\right)^2}{n}} \quad (2)$$

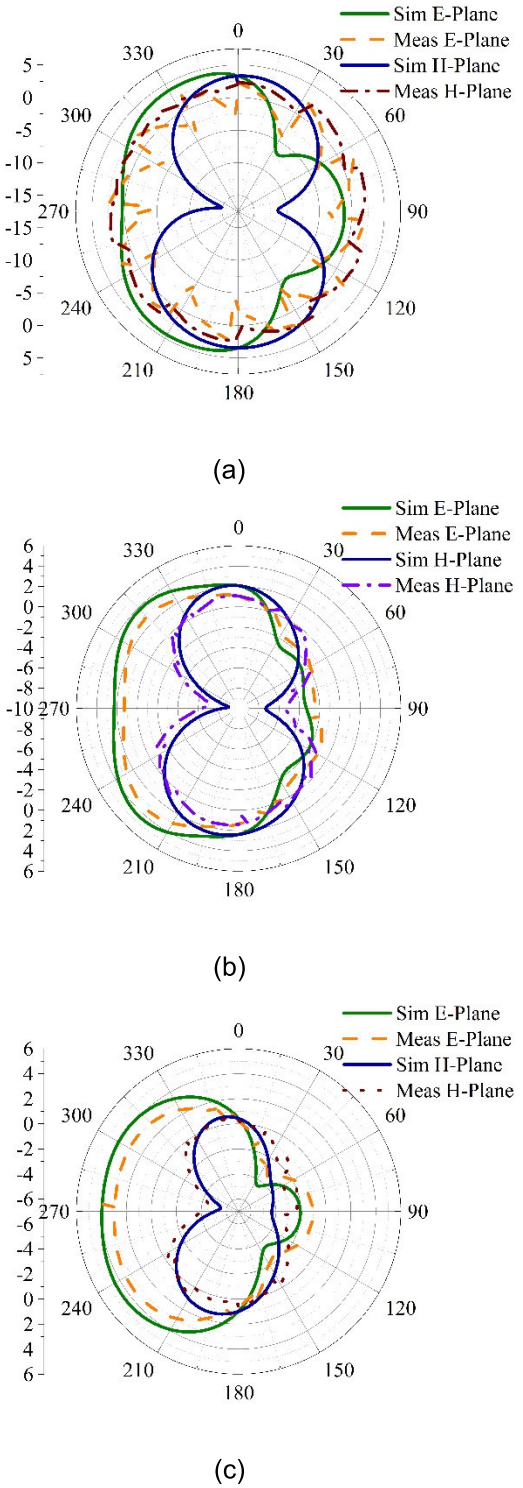

FIGURE 22. Simulation and measurement pattern reconfigurability at 5.8GHz (a) case-00, (b) case-01, and (c) case-02.

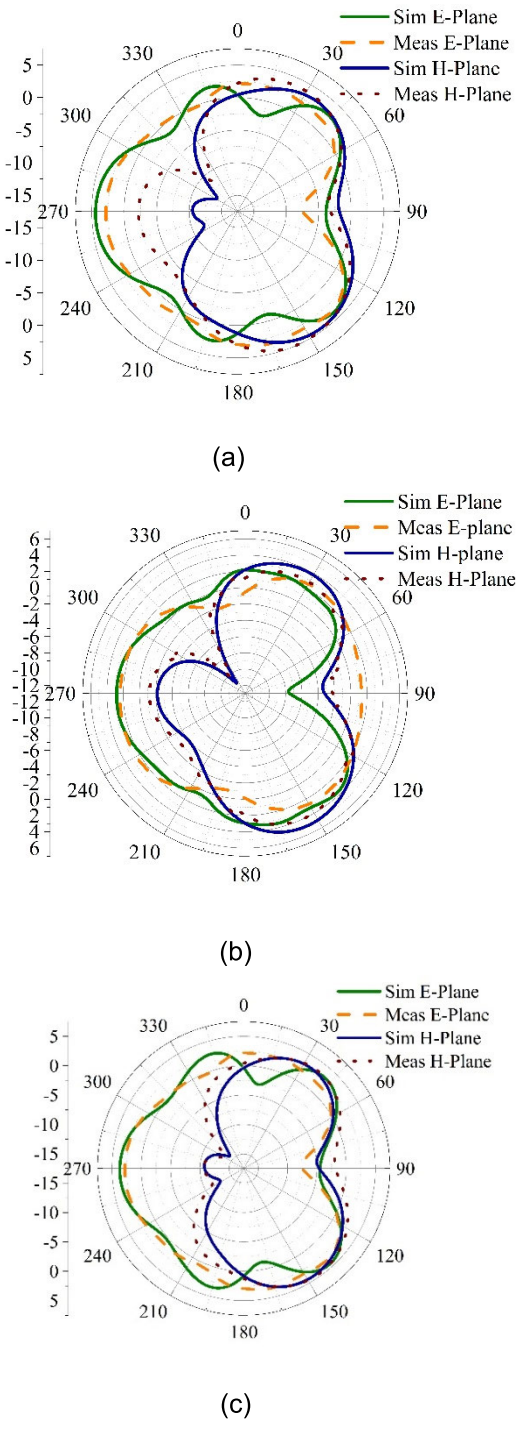

FIGURE 23. Simulation and measurement pattern reconfigurability at 10.5GHz (a) case-00, (b) case-01, and (c) case-02.

The incident wave from port to patch is represented by a_i, and b_i signifies the waves reflected from patch to port. The variable n indicates the count of MIMO elements engaged in transmission or reception. TARC also imparts insights into the observable return loss of the MIMO antenna. The measured and simulated TARC, shown in Figure 27, is below -10 dB, in compliance with established norms. Another gauge of element correlation in the antenna is the ECC, which influences the capacity of the MIMO system's channel. As per standards, the ECC should be below 0.1, as indicated by [34]

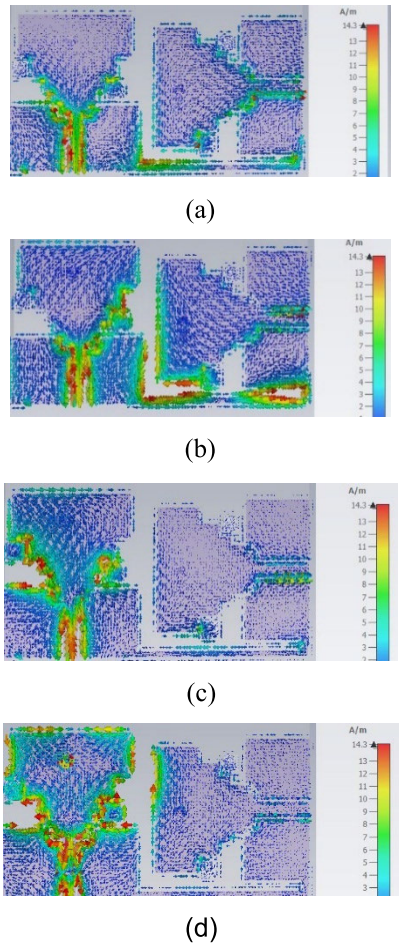

FIGURE 24. Current distribution at (a) 2.8GHz, (b) 3.5GHz, (c) 5.8GHz, and (d) 10.5GHz when port 1 is excited.

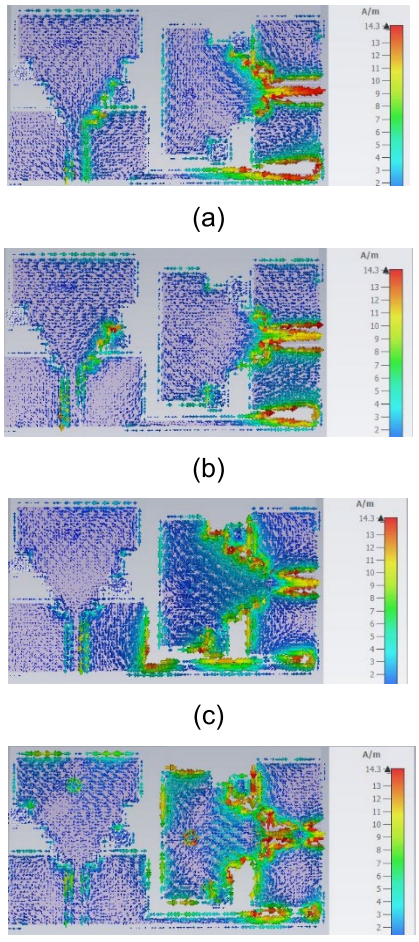

FIGURE 25. Current distribution at (a) 2.8GHz, (b) 3.5GHz, (c) 5.8GHz, and (d) 10.5GHz when port 2 is excited.

and [35]. It can be evaluated using equation (3) [36].

$$\rho e = \frac{\left|\iint_{4\pi}\left[\vec{F}_1(\theta,\phi)\times\vec{F}_2(\theta,\phi)d\Omega\right]\right|^2}{\left|\iint_{4\pi}\left[\vec{F}_1(\theta,\phi)\right]\right|^2 d\Omega\left|\iint_{4\pi}\left[\vec{F}_2(\theta,\phi)\right]\right|^2 d\Omega} \tag{3}$$

The far-field characteristic of the MIMO is denoted by $\vec{F}_i(\theta,\varphi)$ when either port 1 or 2 is stimulated. The alteration in ECC is illustrated in Figure 28, with a measurement below 0.0012.

The diversity gain (DG) serves as an additional performance measure to confirm the extent of power reduction in transmission. It is calculated based on the ECC using the approach outlined in [37].

$$DG = 10\times\sqrt{1-\rho^2} \tag{4}$$

The diversity gain (DG) of the antenna under consideration is 9.994dB, depicted in Figure 29. Increasing the number of antenna elements results in a linear reduction of channel capacity. To effectively accommodate real data rates, MIMO systems benefit from a higher number of antenna elements, resulting in improved channel capacity and a crucially desired decrease in Channel Capacity Loss (CCL). This relationship is depicted in Figure 30, where both measured and simulated CCL can be evaluated through the method

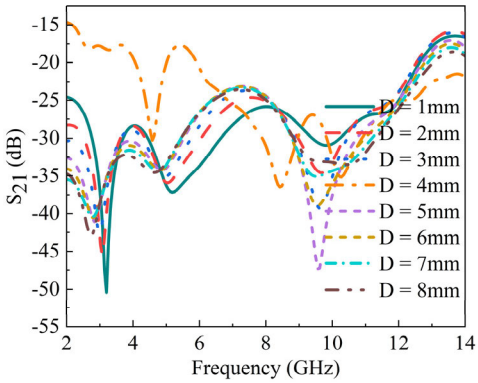

FIGURE 26. Parametric analysis of the distance between the two antennas.

TABLE 6. Comparison of frequency and pattern reconfigurable antenna.

Ref.	Size		Switching technique	Cover band	Bandwidth (GHz or %)	Peak gain (dBi)	Isolation(dB)	Efficiency	BDR
	mm^2	$\lambda_0 \times \lambda_0$							
[7]	21 x 15	0.23 x 0.16	Pin diode	ISM, WiMAX, WLAN WiFi, C	3.3-6 (58.1)	2.04	-	-	1,578.8
[18]	20 x 40	0.1 x 0.2	Varactors	ISM, WiMAX	1.48-4.56 (102.6)	-	18	-	5,130
[19]	52 x 52	0.52 x 0.52	Pin diode	5G, WLAN	2.9-13.8 (200)	6	15.5	-	739.6
[20]	50 x 50	0.51 x 0.51	Pin diode	X, UWB	3.1-12.1 (200)	5.73	18.6	-	768.9
[21]	165 x 85	0.38 x 0.19	Strips	GSM, LTE, UMTS	0.5-3 (200)	-	11	40%	2,770
[22]	50 x 25	0.6 x 0.3	Pin diode	WiMAX, WLAN	3.2-5.7 (200)	2.76	20	88%	1,111.1
[23]	15 x 20	0.17 x 0.23	Varactors	S, 5G, WLAN	3.4-3.8 (221)	2.47	10.2	75%	5,652.1
[24]	100 x 50	0.48 x 0.24	Pin & Var	GSM, LTE, PCS, UMTS, WiMAX	1.42-2.27 (184.5)	2.2	12	78%	1,601.6
[25]	120 x 60	0.36 x 0.18	Pin diode	GSM, WiMAX	0.9-2.6 (175)	3.98	12.5	92.5%	2700.6
[26]	30 x 20	0.38 x 0.25	Varactors	S, C, WLAN, WiMAX	2.4-5.7 (200)	2.46	25	54.72%	2,105.3
[27]	40 x 100	0.33 x 0.83	Pin diode	LTE, WiMAX,	2.5-4.5 (200)	5	10	78%	730.2
This work	**32 x 26**	**0.30 x 0.24**	**Pin diode**	**WLAN, WiMAX, X, 4G, 5G, X**	**2.8 – 14 (240)**	**6.2**	**28**	**82%**	**3,333.3**

described in [38].

$$CCL = -\log_2\left(A^{\rho}\right) \tag{5}$$

where,

$$A^{\rho} = \begin{vmatrix} \rho_{11} & \rho_{12} \\ \rho_{21} & \rho_{22} \end{vmatrix} \tag{6}$$

The effective gain stands as a metric gauging the power received through the diversity antenna relative to the total average power received through the isotropic antenna [39]. The computation of the (MEG) employs the method detailed in [40].

$$MEG = 0.5\left[1 - \sum_{j=1}^{N} \left|S_{ij}\right|^2\right] \tag{7}$$

N denotes the count of antennas, with (i) indicating the input port. The MEG is graphically presented in Figure 31. The proposed MIMO antenna has been compared to other related literature in various aspects, and the comparison is summarized in Table 6. The bandwidth dimensional ratio (BDR) is

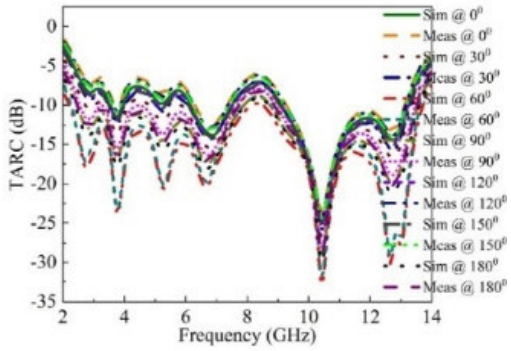

FIGURE 27. Comparison of simulated and measured TARC.

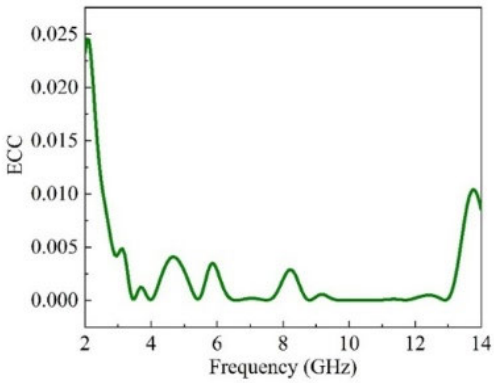

FIGURE 28. Variation of ECC with frequency.

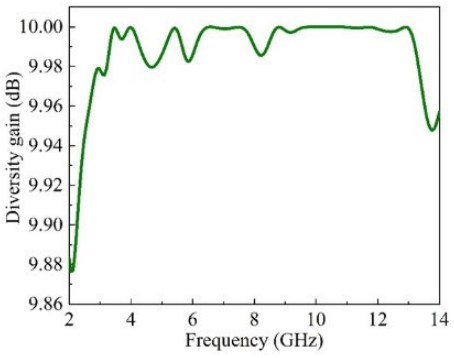

FIGURE 29. Variation of DG with frequency.

computed to measure the antenna's compression, as described in [41].

$$BDR = \frac{\%BW}{\lambda_w \times \lambda_L} \tag{8}$$

Based on the comparison Table, the proposed MIMO antenna has a smaller size than [19, 20, 21, 22, 24, 25 and 27] with a peak realized gain better than most of the referenced works. Furthermore, the proposed antenna has achieved the best isolation, although no decoupling mechanism has been utilized.

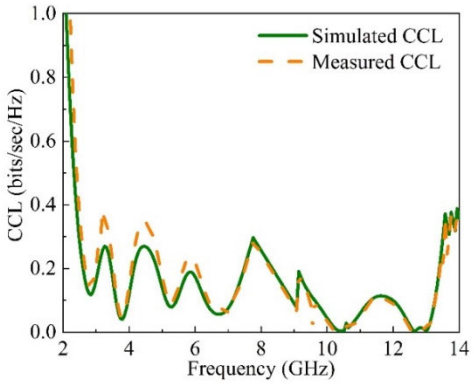

FIGURE 30. Measured and simulated channel capacity loss.

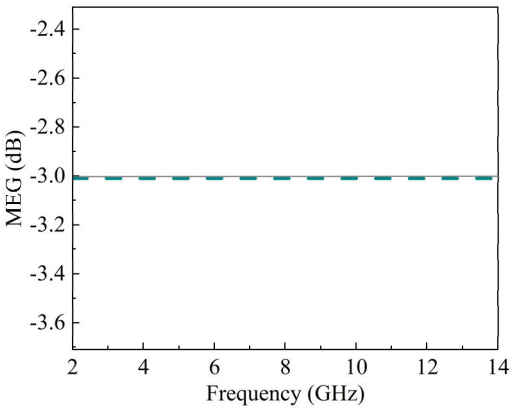

FIGURE 31. Variation of MEG with frequency.

V. CONCLUSION

In this study, a frequency and pattern reconfigurable MIMO antenna is designed and simulated for high gain and efficiency while operating in different frequency bands. Two open-circuited transformers are coupled to a stepped rectangular radiator via diodes D1 – D4. MIMO antennas are capable of tuning four different frequency bands, including WiMAX, WLAN, 4G and X-Band. The pattern reconfigurability can be achieved with competitive results, depending on the activation state of the diodes (ON/OFF). Furthermore, the antenna boasts a maximum gain of 6.2dBi and a radiation efficiency of more than 80%. Also, the antenna shows good MIMO performance and can, therefore, be used in various wireless communication systems.

REFERENCES

[1] M. Gupta, S. Sharma, H. Joshi, and S. J. Darak, "Reconfigurable architecture for spatial sensing in wideband radio front-end," *IEEE Trans. Circuits Syst. II, Exp. Briefs*, vol. 69, no. 3, pp. 1054–1058, Mar. 2022.

[2] A. Kantemur, J. Tak, P. Siyari, A. H. Abdelrahman, M. Krunz, and H. Xin, "A novel compact reconfigurable broadband antenna for cognitive radio applications," *IEEE Trans. Antennas Propag.*, vol. 68, no. 9, pp. 6538–6547, Sep. 2020.

[3] M. Hussain, E. M. Ali, W. A. Awan, N. Hussain, M. Alibakhshikenari, B. S. Virdee, and F. Falcone, "Electronically reconfigurable and conformal triband antenna for wireless communication systems and portable devices," *PLoS ONE*, vol. 17, no. 12, pp. 1–15, 2022.
[4] H. T. Chattha, M. K. Ishfaq, B. A. Khawaja, A. Sharif, and N. Sheriff, "Compact multiport MIMO antenna system for 5G IoT and cellular handheld applications," *IEEE Antennas Wireless Propag. Lett.*, vol. 20, pp. 2136–2140, 2021.
[5] W. A. Awan, N. Hussain, S. A. Naqvi, A. Iqbal, R. Striker, D. Mitra, and B. D. Braaten, "A miniaturized wideband and multiband on-demand reconfigurable antenna for compact and portable devices," *AEU Int. J. Electron. Commun.*, vol. 122, Jul. 2020, Art. no. 153266.
[6] S. Padmanathan, A. Abdullah Al-Hadi, A. M. Elshirkasi, S. S. Al-Bawri, M. T. Islam, T. Sabapathy, M. Jusoh, P. Akkaraekthalin, and P. J. Soh, "Compact multiband reconfigurable MIMO antenna for sub-6 GHz 5G mobile terminal," *IEEE Access*, vol. 10, pp. 60241–60252, 2022.
[7] S. Saleem, S. Kumari, and D. Yadav, "A planar UWB-MIMO antenna with high isolation and reconfigurable single band elimination characteristics," *Int. J. Electron. Commun.*, vol. 170, pp. 1–14, Oct. 2023.
[8] P. Jain and S. Ghosh, "A reconfigurable four-port MIMO antenna for Sub-6 GHz applications," in *Proc. IEEE Wireless Antenna Microw. Symp. (WAMS)*, Rourkela, India, Jun. 2022, pp. 1–5.
[9] R. Hussain, M. U. Khan, and M. S. Sharawi, "Frequency reconfigurable MIMO antenna using SRR for multiband operation," in *Proc. Eur. Conf. Antenna Propag. (EUCAP)*, Krakow, Poland, Mar. 2019, pp. 1–3.
[10] Y. Xu, Y. Tian, and B. Zhang, "A novel RF-MEMS switch on frequency reconfigurable antenna application," *Microsyst. Technol.*, vol. 24, pp. 3833–3841, Sep. 2018.
[11] R. Shanmugam, "Design and analysis of a frequency reconfigurable pentaband antenna for WLAN and 5G applications," *J. Electromagn. Eng. Sci.*, vol. 21, no. 3, pp. 228–235, Jul. 2021.
[12] V. Choudhary, M. K. Meshram, and J. Hesselbarth, "Four elements reconfigurable MIMO antenna for dual band applications," *Int. J. Adv. Microw. Technol.*, vol. 7, no. 1, pp. 274–282, 2022.
[13] V. Mohadesi, A. Asgari, V. Siahpoush, and S. S. Taheri, "Analysis and optimization of graphene-based reconfigurable electro-optical switches," *Micro Nanostruct.*, vol. 165, May 2022, Art. no. 207193.
[14] L. Vallejo, B. Ortega, J. Bohata, S. Zvanovec, and V. Almenar, "Photonic multiple millimeter wave signal generation and distribution over reconfigurable hybrid SSMF/FSO links," *Opt. Fiber Technol.*, vol. 54, Jan. 2020, Art. no. 102085.
[15] D. E. Anagnostou, D. Torres, T. S. Teeslink, and N. Sepulveda, "Vanadium dioxide for reconfigurable antennas and microwave devices: Enabling RF reconfigurability through smart materials," *IEEE Antennas Propag. Mag.*, vol. 62, no. 3, pp. 58–73, Jun. 2020.
[16] P. Sanchez-Olivares, J. L. Masa-Campos, A. T. Muriel-Barrado, R. Villena-Medina, and G. M. Fernandez-Romero, "Mechanically reconfigurable linear array antenna fed by a tunable corporate waveguide network with tuning screws," *IEEE Antennas Wireless Propag. Lett.*, vol. 17, pp. 1430–1434, 2018.
[17] A. M. Sadiq, Y. Gu, Y. Luo, Y. Chen, and K. Ma, "Gain-enhanced reconfigurable radiation array with mechanically driven system and directive elements," *Frontiers Mech. Eng.*, vol. 17, no. 4, pp. 1–19, Dec. 2022.
[18] R. Hussain and M. S. Sharawi, "An integrated slot-based frequency-agile and UWB multifunction MIMO antenna system," *IEEE Antennas Wireless Propag. Lett.*, vol. 18, pp. 2150–2154, 2019.
[19] S. Sumayya, K. Sarita, Y. Danesh, and B. Deepak, "Frequency reconfigurable MIMO antenna for ultra-wideband applications," in *Proc. IEEE Indian Conf. Antennas Propag. (INCAP)*, Jaipur, India, Sep. 2021, pp. 816–819.
[20] T. Durukan and Y. Altuncu, "A compact 4×4 reconfigurable MIMO antenna design with adjustable suppression of certain frequency bands within the UWB frequency range," *Int. J. Electron. Commun.*, vol. 170, pp. 1–10, Oct. 2022.
[21] S. Saleem, S. Kumari, D. Yadav, and D. Bhatnagar, "Frequency reconfigurable MIMO (multiple-input multiple-output) antenna for ultrawideband applications," in *Proc. IEEE Indian Conf. Antennas Propag. (InCAP)*, Dec. 2021, pp. 816–819.
[22] P. S. Rathore, R. Mali, R. Jatav, and M. K. Meshram, "Integrated UWB and frequency reconfigurable antenna with high isolation for cognitive radio," *Int. J. Electron. Commun.*, vol. 171, pp. 1–11, Nov. 2023.
[23] A. K. Singh, S. K. Mahto, P. Kumar, R. K. Mistri, and R. Sinha, "Reconfigurable circular patch MIMO antenna for 5G (sub-6 GHz) and WLAN applications," *Int. J. Commun. Syst.*, vol. 35, no. 16, Nov. 2022, Art. no. e5313.
[24] S. Nej, A. Ghosh, J. Kumar, and S. Das, "Ultra-wideband MIMO antenna with reconfigurable band notch characteristics and improved isolation," *AEU Int. J. Electron. Commun.*, vol. 170, Oct. 2023, Art. no. 154849.
[25] X. Zhao, S. Riaz, and S. Geng, "A reconfigurable MIMO/UWB MIMO antenna for cognitive radio applications," *IEEE Access*, vol. 7, pp. 46739–46747, 2019.
[26] X. Li and H. Xu, "A compact dual trap reconfigurable ultra-wideband MIMO antenna design," in *Proc. 4th Int. Symp. Comput. Eng. Intell. Commun. (ISCEIC)*, Aug. 2023, pp. 466–471.
[27] S. S. Jehangir, R. Hussain, M. I. Hussein, and M. S. Sharawi, "Frequency reconfigurable Yagi-like MIMO antenna system with a wideband reflector," *IET Microw., Antennas Propag.*, vol. 14, no. 7, pp. 586–592, Jun. 2020.
[28] A. M. Montaser, "Machine learning based design of pattern reconfigurable antenna," *IEEE Access*, vol. 11, pp. 33121–33133, 2023.
[29] C. J. You, S. H. Liu, J. X. Zhang, X. Wang, Q. Y. Li, G. Q. Yin, and Z. G. Wang, "Frequency and pattern reconfigurable antenna array with broadband tuning and wide scanning angle," *IEEE Trans. Antennas Propag.*, vol. 71, no. 6, pp. 5398–5403, Jun. 2023.
[30] J. Hao, J. Ren, X. Du, J. H. Mikkelsen, M. Shen, and Y. Z. Yin, "Pattern-reconfigurable Yagi–Uda antenna based on liquid metal," *IEEE Antennas Wireless Propag. Lett.*, vol. 20, pp. 587–591, 2021.
[31] S. Zhao, Z. Wang, and Y. Dong, "Pattern-reconfigurable antenna using low-profile electric and magnetic radiators," *IEEE Antennas Wireless Propag. Lett.*, vol. 22, pp. 616–620, 2023.
[32] Y. Faouri, S. Ahmad, S. Naseer, K. Alhammami, N. Awad, A. Ghaffar, and M. I. Hussein, "Compact super wideband frequency diversity hexagonal shaped monopole antenna with switchable rejection band," *IEEE Access*, vol. 10, pp. 42321–42333, 2022.
[33] P. Pannu and D. K. Sharma, "Miniaturize four-port UWB-MIMO antenna with tri-notched band characteristics," *Microw. Opt. Technol. Lett.*, vol. 63, no. 5, pp. 1489–1498, May 2021.
[34] G. Saxena, S. Chintakindi, M. A. Kasim, P. K. Maduri, Y. K. Awasthi, S. Kumar, S. Kansal, R. Jain, M. K. Sharma, and C. Dewan, "Metasurface inspired wideband high isolation THz MIMO antenna for nano communication including 6G applications and liquid sensors," *Nano Commun. Netw.*, vol. 34, Dec. 2022, Art. no. 100421.
[35] G. Saxena, Y. K. Awasthi, and P. Jain, "Design of metasurface absorber for low RCS and high isolation MIMO antenna for radio location and navigation," *Int. J. Electron. Commun.*, vol. 133, pp. 1–10, May 2021.
[36] A. Iqbal, A. Smida, A. J. Alazemi, M. I. Waly, N. K. Mallat, and S. Kim, "Wideband circularly polarized MIMO antenna for high data wearable biotelemetric devices," *IEEE Access*, vol. 8, pp. 17935–17944, 2020.
[37] S. H. Ghadeer, S. K. A. Rahim, M. Alibakhshikenari, B. S. Virdee, T. A. Elwi, A. Iqbal, and M. Al-Hasan, "An innovative fractal monopole MIMO antenna for modern 5G applications," *AEU Int. J. Electron. Commun.*, vol. 159, Feb. 2023, Art. no. 154480.
[38] A. Mohanty and S. Sahu, "A micro four port THz MIMO antenna for nano communication networks," *Photonic Nanostruct. Fundam. Appl.*, vol. 53, pp. 1–14, Feb. 2023.
[39] V. Puri and H. S. Singh, "Design of an isolation improved MIMO antenna using metasurface based absorber for wireless applications," *Optik*, vol. 259, Jun. 2022, Art. no. 168963.
[40] S. Jabeen and Q. U. Khan, "An integrated MIMO antenna design for sub-6 GHz and millimeter-wave applications with high isolation," *Int. J. Electron. Commun.*, vol. 153, pp. 1–10, Aug. 2022.
[41] D. Lodhi and S. Singhal, "CPW fed shovel shaped super wideband MIMO antenna for 5G applications," *AEU Int. J. Electron. Commun.*, vol. 168, Aug. 2023, Art. no. 154700.

ADAMU HALILU JABIRE (Member, IEEE) was born in Jalingo, Taraba, Nigeria. He received the B.Eng. degree in electrical and electronics engineering from Ahmadu Bello University Zaria, Nigeria, in 2010, the M.Eng. degree in signal and information processing from Tianjin University of Technology and Education, China, in 2015, and the Ph.D. degree in electronics and information engineering from Hebei University of Technology, China, in 2020. His research interests include wireless communication and modeling of microwave circuits and antennas, reconfigurable antennas, MIMO antennas, metamaterial antennas, and sensors.

HAMAD M. ALKHOORI (Member, IEEE) received the B.S. degree in electrical engineering from United Arab Emirates University, in 2013, and the M.S. and Ph.D. degrees in electrical engineering from Pennsylvania State University, in 2016 and 2019, respectively. He is currently an Assistant Professor of electrical engineering with United Arab Emirates University. His research interest includes electromagnetic scattering.

ADNAN GHAFFAR received the B.Sc. degree in computer engineering from Bahauddin Zakariya University (BZU), Multan, Pakistan, in 2010, the M.E. degree in circuits and systems from Lanzhou Jiaotong University, Lanzhou, China, in 2015, and the Ph.D. degree in electrical and electronics engineering from Auckland University of Technology, Auckland, New Zealand. His research interests include RF circuits, reconfigurable antennae, embedded systems, metasurface antennae, and flexible and wearable antenna design.

YANAL S. FAOURI (Senior Member, IEEE) received the B.Sc. degree in electrical engineering from The University of Jordan, Amman, Jordan, in 2007, and the M.Sc. and PhD. degrees in electrical engineering from the King Fahd University of Petroleum and Minerals (KFUPM), Dhahran, Saudi Arabia, in 2010 and 2014, respectively.

In 1997, he joined the Faculty of Engineering, Amman University, Amman, as an Assistant Professor. He joined the Department of Electrical Engineering, Philadelphia University, in 2014. Since September 2015, he has been a Faculty Member with the Department of Electrical Engineering, The University of Jordan.

ABDULRAHMAN DAHIR received the B.S. and M.S. degrees in electrical engineering from United Arab Emirates University, in 2004 and 2011, respectively. In 2006, he joined United Arab Emirates University as a Teaching Assistant. He has been a Laboratory Specialist with the High-Frequency Laboratory, since 2011, where he is responsible for the characterization of RF devices.

MOUSA I. HUSSEIN (Senior Member, IEEE) received the B.Sc. degree in electrical engineering from West Virginia Tech, Montgomery, WV, USA, in 1985, and the M.Sc. and Ph.D. degrees in electrical engineering from the University of Manitoba, Winnipeg, Canada, in 1992 and 1995, respectively. From 1995 to 1997, he was with the Research and Development Group, Integrated Engineering Software Inc., Winnipeg, working on developing EM specialized software based on the boundary element method. In 1997, he joined the Faculty of Engineering, Amman University, Amman, Jordan, as an Assistant Professor. He is currently a Professor with the Department of Electrical Engineering, United Arab Emirates University. He has more than 100 publications in international journals and conferences. He has supervised several M.Sc. and Ph.D. students. His current research interests include computational electromagnetics, electromagnetic scattering, antenna analysis and design, metamaterial and applications, material/bio-material characterization, and sensor design for bio applications.